University of California Transportation Center
UCTC-FR-2012-09

Development and Evaluation of Intelligent Energy Management Strategies for Plug-in Hybrid Electric Vehicles

Guoyuan Wu,
Kanok Boriboonsomsin, and
Matthew Barth,
UC Riverside
May 2012

Development and Evaluation of Intelligent Energy Management Strategies for Plug-in Hybrid Electric Vehicles

Guoyuan Wu, Ph. D
CE-CERT, University of California at Riverside
1084 Columbia Ave, Riverside, CA 92507, USA
Tel: (951) 781-5630, Fax: (951) 781-5790
E-mail: gywu@engr.ucr.edu

Kanok Boriboonsomsin, Ph. D., P. E.
CE-CERT, University of California at Riverside
1084 Columbia Ave, Riverside, CA 92507, USA
Tel: (951) 781-5792, Fax: (951) 781-5790
E-mail: kanok@cert.ucr.edu

Matthew Barth, Ph. D.
CE-CERT, University of California at Riverside
1084 Columbia Ave, Riverside, CA 92507, USA
Tel: (951) 781-5782, Fax: (951) 781-5790
E-mail: barth@cert.ucr.edu

ABSTRACT

In this study, we proposed an intelligent energy management strategy for plug-in hybrid electric vehicles. At the trip level, the strategy takes into account a priori knowledge of vehicle location, roadway characteristics, and real-time traffic information on the travel route from intelligent transportation system technologies in generating synthesized velocity trajectory for the trip. The synthesized velocity trajectory is then used to determine charge-depleting control that is formulated as a mixed integer linear programming to minimize the total fuel consumption for the trip. The strategy can be extended to optimize fuel consumption at the tour level if a pre-planned travel itinerary for the tour and the information about available battery recharging opportunities at intermediate stops in the tour are available. The effectiveness of the proposed strategy, both for the trip-based and tour-based controls, was evaluated against the existing binary mode energy management strategy using a real-world example trip/tour in Southern California. The evaluation results show that the fuel savings of the proposed strategy over the binary mode strategy are around 10-15%.

Keywords:
Plug-in hybrid electric vehicle, intelligent transportation system, optimization, fuel consumption

INTRODUCTION

Transportation-related energy consumption and air quality degradation have been a major concern for years. In the United States, the total energy consumption by the transportation sector was estimated to be as high as 27.51 Quadrillion Btu in 2010 (*1*), and the U.S. Environmental Protection Agency (EPA) reported that nearly 33% of carbon dioxide (CO_2) emissions, 24% of methane (CH_4) emission, and 65% of nitrous oxide (N_2O) emissions resulted from fossil fuel combustion for transportation activities in 2009 (*2*).

Numerous technologies and strategies have been developed and deployed to address these energy and environment issues. Among those, advanced vehicle technologies, such as hybrid electric vehicles (HEVs) and electric vehicle (EVs), are very promising in improving fuel efficiency of motor vehicles. As one type of HEVs, plug-in hybrid electric vehicles (PHEVs) can be plugged into the electrical grid to charge its battery, thus increasing the use of electrical energy and achieving even higher overall fuel efficiency (*3*).

One of the critical considerations in PHEV development is the design of the energy management strategy, which determines how energy in a hybrid powertrain should be produced and utilized as a function of various vehicle parameters. In the past decade, a variety of energy management strategies for PHEVs have been developed from control and optimization perspectives (*4-8*). Most of these strategies were evaluated using standard driving cycles such as the EPA's city and highway cycles for fuel economy testing. Thus, their effectiveness under real-world driving conditions (e.g., traffic congestion and road topology) was unknown. In addition, to our best knowledge, PHEV energy management studies to date have only focused on optimizing energy consumption for individual trips without considering recharging opportunities (e.g., at workplace or shopping malls) in the trip chain or tour where additional fuel saving benefits can be gained from the plug-in capability of PHEVs.

Therefore, in this study we proposed an intelligent energy management strategy for PHEVs. At the trip level, the strategy takes into account *a priori* knowledge of vehicle location, roadway characteristics, and real-time traffic information on the travel route from intelligent transportation system (ITS) technologies to determine charge-depleting control that minimizes fuel consumption for the trip. The strategy can also be extended to optimize energy consumption at the tour level if a pre-planned travel itinerary for the tour and the information about available battery recharging opportunities at intermediate stops in the tour are available. The effectiveness of the proposed strategy was evaluated against existing strategies using a real-world case study.

BACKGROUND

To develop an intelligent energy management strategy for PHEVs, we need to first be able to estimate the required power at the wheels on a continuous basis. Therefore, second-by-second velocity trajectories for individual trips need to be synthesized based on roadway characteristics (e.g., road grade) and real-time traffic information (e.g., average traffic speed) on the travel route. These synthetic velocity trajectories are then used in conjunction with PHEV vehicle and powertrain models to determine the optimal energy management strategy.

Velocity Trajectory Synthesis

Numerous studies have been conducted to estimate vehicle speed or reconstruct velocity trajectory using real-world traffic data collected from various surveillance systems, in particular the prevalent inductive loop detectors (ILD). Based on 5-minute ILD data, Chen et al. (*9*) proposed to used traffic speed at the closest loop detector during the closest time interval as the estimate of instantaneous speed, while Rice and Van Zwet (*10*) suggested to use the average speed between two bracketing ILDs as a surrogate. Ni and Wang (*11*) proposed a two-dimensional interpolation method to reconstruct velocity trajectories based on point-based speed data collected by existing intelligent transportation systems (ITS). Krol (*12*) evaluated two different models, one data-driven and the other based on fundamental-diagram (FD), for synthesizing velocity trajectory using dynamic macroscopic traffic data. Besides point-based detection data, Herrera and Bayen (*13*) integrated probe-vehicle data to reconstruct traffic states, which could be further used for trajectory synthesis. Barth et al. (*14*) set up models to relate the statistics of microscopic traffic data with macroscopic flow, speed, and density parameters under different traffic conditions. Lin and Niemeier (*15*) proposed a statistical approach to construct driving cycles (i.e., velocity trajectories) based on segmented microscopic data with specific modal operating conditions, such as cruise, idle or acceleration/deceleration).

PHEV Modeling and Energy Management

Numerous studies have been conducted to model hybrid electric vehicles (HEV) or Plug-in Hybrid Electric Vehicle (PHEV) (*16*, *17*). The modeling approaches can be categorized into two types with respect to the physical causality principles (*18*):

1) Forward approach. It is assumed that the command signals proceed from the driver to the wheel. This approach takes the driver commands as inputs, models the physical behavior of each component, and generates the vehicle performance as outputs.
2) Backward approach. It is assumed that a) the vehicle can meet the target performance at each time step; b) the vehicle velocity profile is predetermined; and c) the required power can be calculated using the kinematic relationship imposed by the drivetrain.

Compared with the forward modeling approach, the backward one is less complicated, due to not having to solve the differential motion equations for the vehicle. However, the former seems to be more appropriate for real-world implementation since it reflects the actual system architecture and command signal direction.

A variety of HEV or PHEV energy management strategies have been proposed and evaluated in previous studies for different purposes (*19*-*25*). These strategies can be grouped into two categories:

1) Binary mode (e.g., CD-CS). In this strategy, the vehicle operates in charge depleting (CD) mode as long as the electric motor(s) can supply the required power and the state of charge (SOC) of battery pack is higher than a minimum threshold. Once the battery depletes to the minimum SOC, the vehicle switches to charge sustaining (CS) mode.
2) Blended mode. In this strategy, the internal combustion engine (ICE) is used in

conjunction with the electric motor(s) along the entire driving cycle. The power splits between ICE and motor(s) are optimized such that the SOC decreases during the trip and reaches the minimum threshold only at the end of the trip.

The blended mode requires a priori knowledge of the driving cycle for the development of charge-depleting control algorithms. Example strategies under this category include:

1) Rule-based strategy. This strategy uses pattern recognition techniques to classify the actual driving cycle into different scenarios and applies a variety of heuristic rules for energy management.
2) Dynamic programming (DP) or stochastic dynamic programming (SDP) strategy. The problem is posed as a multi-stage process requiring a sequence of interrelated decisions (with constraints), and solved by a DP approach. If uncertainties or randomness on the trip information are introduced, the problem can then be formulated as a location-dependent Markov chain with finite horizon, which can be solved by a SDP approach.
3) Equivalent consumption minimization strategy (ECMS) or adaptive equivalent consumption minimization strategy (A-ECMS). Rather than considering the global criterion, this strategy minimizes the instantaneous cost function (i.e., dependent on the system variables at the current time) as a sum of the fuel consumption and an equivalent fuel consumption related to the SOC variation. Such simplified strategy can be well applied in real-time although no global optimum can be guaranteed. However, the performance of this strategy largely depends on the choice of equivalence factor, which may be varied by driving conditions.

In this study, we proposed a novel mixed integer linear programming (MILP) to achieve an optimal charge-depleting control for PHEV. Such an optimization problem can be solved very efficiently for global optimum by commercial solvers.

VELOCITY TRAJECTORY SYNTHESIS METHOD

In this study, vehicle velocity trajectory is synthesized in two steps. First, an initial velocity trajectory is created based on macroscopic traffic data measured by ILDs. This velocity trajectory will have a correct average velocity trend, but can be unrealistically smooth. Thus, in the second step the variation in velocity at the microscopic level is stochastically introduced using representative driving cycles for the corresponding average velocity. It is noted that the implementation of PHEV energy management strategies typically requires prior knowledge of the driving conditions (in terms of anticipated velocity trajectory and the associated road grade information) to calculate the required power for the PHEV. Based on traffic information along the desired route and representative vehicle trajectory datasets used by the U.S. Environmental Protection Agency (EPA) in their Motor Vehicle Emission Simulator (MOVES) model (*26*), a synthesized velocity trajectory of the subject vehicle can be written as

$$v(t) = v'(t) + v''(t) \quad (1)$$

where $v(t)$ is the synthesized instant velocity at time *t*; $v'(t)$ is the average velocity of traffic at time *t*; and $v''(t)$ is the random variation in velocity for the subject vehicle at time *t*.

To reconstruct each component of the right hand side of Equation (1), we employed the following methods: a) average velocity estimation using 2-D interpolation; and b) random velocity disturbance generation based on representative driving cycles.

Average Velocity Estimation Using 2-D Interpolation

In this study, we proposed a two-dimensional interpolation method which has been modified based on (*11*), to estimate the velocity of average traffic based on aggregated data (e.g., 5-minute) from vehicle detector stations (VDS).

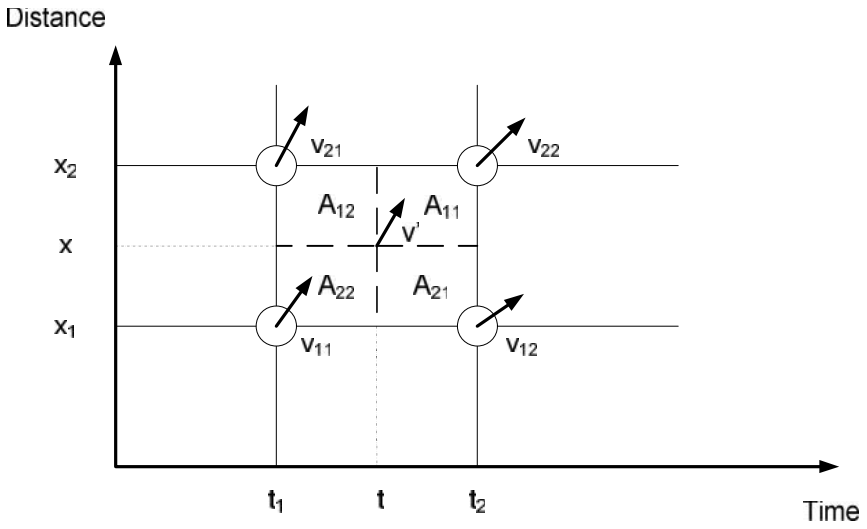

FIGURE 1 Illustration of velocity estimation using 2-D interpolation method.

As illustrated in Figure 1, suppose that there are two VDSs located at x_1 and x_2, respectively. Then, the estimated velocity of average traffic at time t and location x can be written as,

$$v'(x,t) = \frac{A_{11} \cdot v_{11} + A_{12} \cdot v_{12} + A_{21} \cdot v_{21} + A_{22} \cdot v_{22}}{A_{11} + A_{12} + A_{21} + A_{22}} \qquad \forall x \in (x_1, x_2) \text{ and } t \in (t_1, t_2) \tag{2}$$

where v_{ij} represents the aggregated velocity measurement at (x_i, t_j); and A_{ij}'s denote the associated "areas" in the 2-D plane. However, this method only uses simple mathematical relationship but no traffic flow theory.

Alternatively, the velocity estimation method in this study can be divided into two steps. First, we apply the same 2-D interpolation technique to estimate both flow, q, and density, k, at (x_i, t_j). Then, we calculate the velocity based on the fundamental relationship

$q = kv$ in traffic flow theory. More specifically, the estimated flow and density of average traffic at time t and location x can be written as

$$q'(x,t) = \frac{A_{11}\cdot q_{11}+A_{12}\cdot q_{12}+A_{21}\cdot q_{21}+A_{22}\cdot q_{22}}{A_{11}+A_{12}+A_{21}+A_{22}} \quad \forall x \in (x_1, x_2) \text{ and } t \in (t_1, t_2) \qquad (2'a)$$

and

$$k'(x,t) = \frac{A_{11}\cdot k_{11}+A_{12}\cdot k_{12}+A_{21}\cdot k_{21}+A_{22}\cdot k_{22}}{A_{11}+A_{12}+A_{21}+A_{22}} \quad \forall x \in (x_1, x_2) \text{ and } t \in (t_1, t_2) \qquad (2'b)$$

where $k_{ij} = q_{ij}/v_{ij}$. Therefore, $v'(x,t)$ can be expressed by harmonic mean as

$$v'(x,t) = \frac{q'(x,t)}{k'(x,t)} = \frac{1}{\sum_{i,j}\frac{\omega_{ij}}{v_{ij}}} \qquad (2')$$

where

$$\omega_{ij} = \frac{A_{ij}\cdot q'_{ij}}{\sum_{i,j} A_{ij}\cdot q'_{ij}}$$

Random Velocity Disturbance Generation Based on Representative Driving Cycles

As aforementioned, $v'(x,t)$ is an estimated average velocity of traffic, which can be unrealistically smooth for the estimation of vehicle energy consumption or emissions. A heuristic way of addressing this issue is to add a random term $v''(x,t)$, e.g., white noise with predetermined variance, to make the velocity trajectory more realistic for an individual vehicle.

In this study, we proposed a method to account for the velocity disturbance of an individual vehicle based on vehicle dynamics of specific vehicle types (passenger cars in our study) under different traffic conditions, extracted from representative driving cycles used by the EPA in their MOVES model (*26*). Examples of representative driving cycles for passenger cars are shown in Figure 2.

Selection of Driving Cycles

To determine which driving cycles are appropriate for extracting vehicle dynamics, the estimate of route velocity, v^R, needs to be obtained first.

Suppose the duration of a whole trip is $N \cdot \Delta t$, where N is the total number of time steps and Δt is the length of each step (e.g., 1 second). If the average traffic velocity at multiple ILDs along the route at each time step is available, then one candidate estimate of the route velocity will be

$$v^R = \frac{1}{N+1}\sum_{t=0}^{N\cdot\Delta t} v'(x,t) \qquad (3)$$

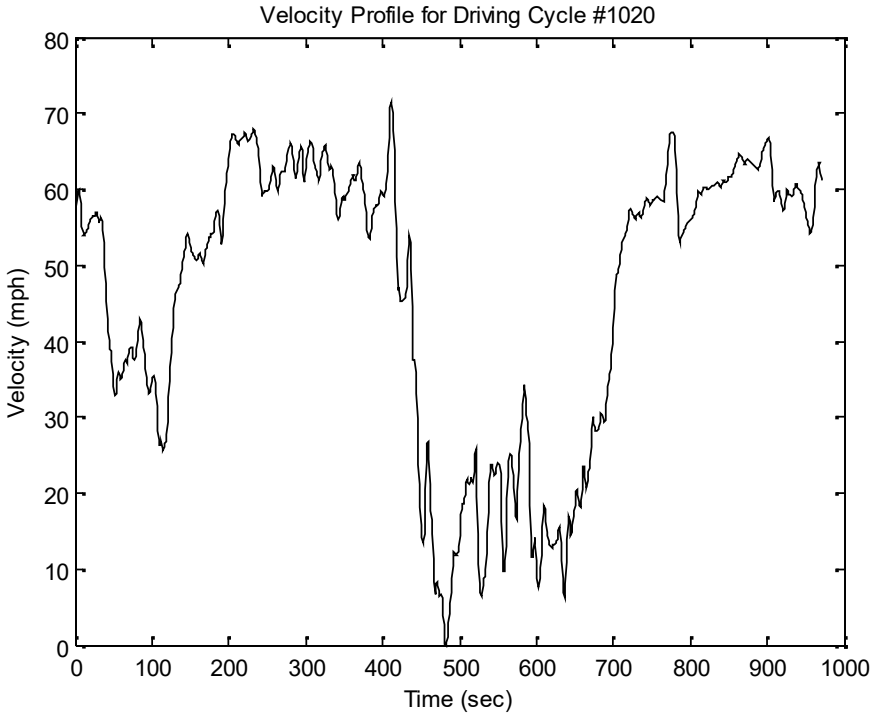

(a) Average speed 46.1 mph

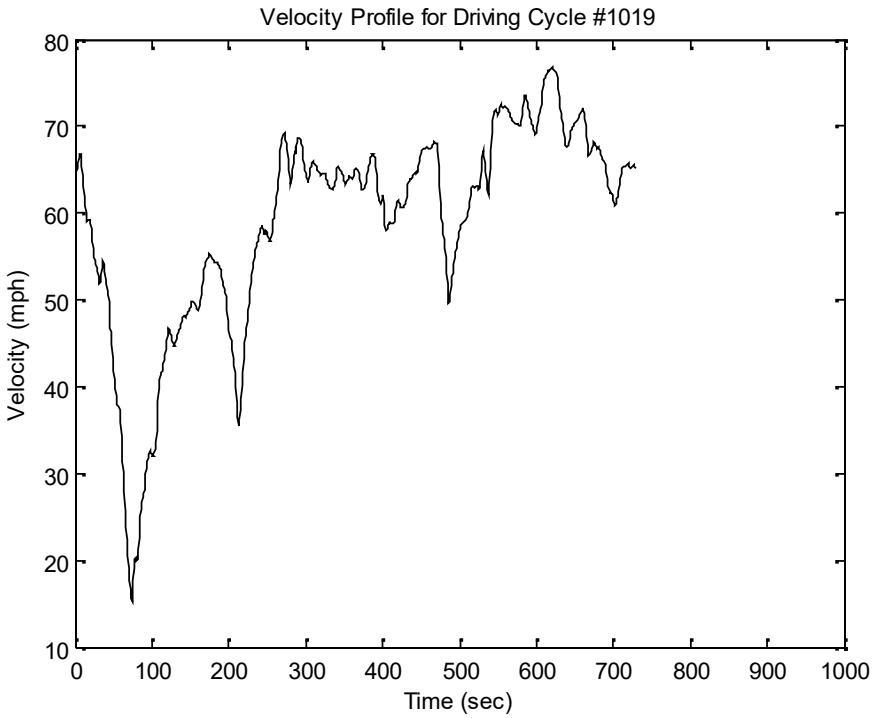

(b) Average speed 58.8 mph

FIGURE 2 Examples of representative driving cycles for passenger cars

However, in the actual implementation, $v'(x,t)$ for any $t > k \cdot \Delta t$ is not available at time $t = k \cdot \Delta t$. Therefore, an alternative of such estimate will be

$$v^R(t) = \frac{1}{k+1} \sum_{t=0}^{k \cdot \Delta t} v'(x,t) \quad (4)$$

or even,

$$v^R(t) = v'(x,t) \quad (5)$$

Based on the estimated route velocity, two driving cycles whose average speeds are the closet to the estimated route velocity and bracket it are selected as sample pools for random velocity disturbance generation. For example, if the estimated route velocity is 50 mph, then Driving Cycles #1020 (average speed of 46.1 mph) and #1019 (average speed of 58.8 mph) are selected. Note that only freeway driving cycles have been considered in this study, but the method can also be applied to non-freeway driving cycles.

After two candidate driving cycles are determined, a target driving cycle is randomly chosen where the probability of selecting which of the two cycles is governed by the difference between the estimated route velocity and the average speed of each driving cycle. For the same example mentioned above, the probability of choosing Driving Cycle #1020 is 0.693 while 0.307 for the other. So, Driving Cycle #1020 is more likely to be selected as the target sample pool.

2-D Binning for Target Driving Cycles

Upon the selection of target driving cycle, data samples are binned based on the joint distribution of velocities at two consecutive time steps. In general, the bin size could be varying, but in this study, we use a fixed bin size of 2 mph for simplicity. Accordingly, acceleration/deceleration value at each time step can be calculated by applying the Central Difference Method to the velocity data.

Random Sampling from Matched Bin

Based on the disturbed velocity at time step k, $v(x_k, t_k)$, and the estimated average velocity of traffic at time step $k+1$, $v'(x_{k+1}, t_{k+1})$, a matched bin can be obtained from the data samples of target driving cycle. Then, an estimated acceleration can be randomly sampled from the selected bin and used to calculate the disturbed velocity at time $t = (k+1) \cdot \Delta t$. Therefore, the synthesized velocity at time t_{k+1} is given by

$$v_{k+1} = \begin{cases} v'_{k+1}, & matched\ bin\ is\ empty \\ v_k + a_k, & otherwise \end{cases} \quad (6)$$

where $a_k = f(v'_k, v'_{k+1})$ and f is the operator which follows the aforementioned procedures to randomly generate a_k using values of $v'(x_k, t_k)$ and $v'(x_{k+1}, t_{k+1})$. In other words,

$$v''_{k+1} = \begin{cases} 0, & matched\ bin\ is\ empty \\ v_k + a_k - v'_{k+1}, & otherwise \end{cases} \quad (7)$$

Care needs to be taken when selecting an acceleration sample from the associated bin which is comparable to the disturbed velocity at time step k, $v(x_k, t_k)$, and estimated velocity at time step $k+1$, $v'(x_{k+1}, t_{k+1})$. Otherwise, the disturbed velocity may drift out of the range of target driving cycles. It should be also mentioned that when implementing the algorithm, we set $v''_0 = 0$.

Flow Chart of Proposed Algorithm

In summary, the synthesized velocity trajectory of a vehicle is governed by the estimated traffic condition (average velocity of traffic) based on real-world data collected from VDS. However, the estimated average velocity of traffic using 2-D interpolation is unrealistically smooth for the estimation of vehicle fuel consumption and emission. Thus, random noise has been introduced to the initial velocity trajectory using vehicle dynamics information under different traffic conditions based on a set of representative driving cycles.

Without loss of generality, we assume that at time $t = 0$, the travel route is known (e.g., it can be generated by the in-vehicle navigation system given starting and ending locations) and the traffic data (e.g., flow, occupancy, and speed) are available from VDS. The flow chart of the proposed algorithm for synthesizing velocity trajectory is presented in Figure 3. In the flow chart, x_k represents the estimated location based on the estimated average velocity of traffic at time $t = k$ (assuming $\Delta t = 1$ sec); y_k is the calculated location of the subject vehicle; v_k is the synthesized velocity at time $t = k$; v'_k is the estimated average velocity of traffic; v_k^R is the estimated route velocity; and $d(> 0)$ is the total travel distance.

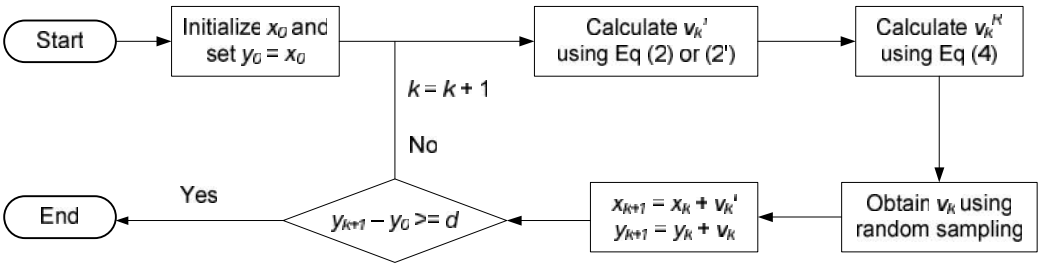

FIGURE 3 Flow chart of the proposed algorithm for vehicle velocity trajectory synthesis.

It should be pointed out that the 2-D interpolation technique is good for estimation but not for prediction of average velocity of traffic. Short-term traffic prediction methods such as those proposed in (*10, 27*) may be used for real-time implementation. In addition, the proposed binning strategy is preliminary and the size of velocity bin (2 mph in this study) may affect the estimation of the random term. Further investigation on the binning strategy can be a potential research topic in the future.

An Example of Synthesized Velocity Trajectory

By following the aforementioned procedures, velocity trajectory can be synthesized for a trip starting at a specified time along a specified route. Figure 4 shows an example trip along I-210 E from the interchange between I-210 and I-605 to Day Creek Blvd. in Southern California, and Figure 5 presents the synthesized velocity trajectory for the trip starting at 16:00 on January 17th, 2012.

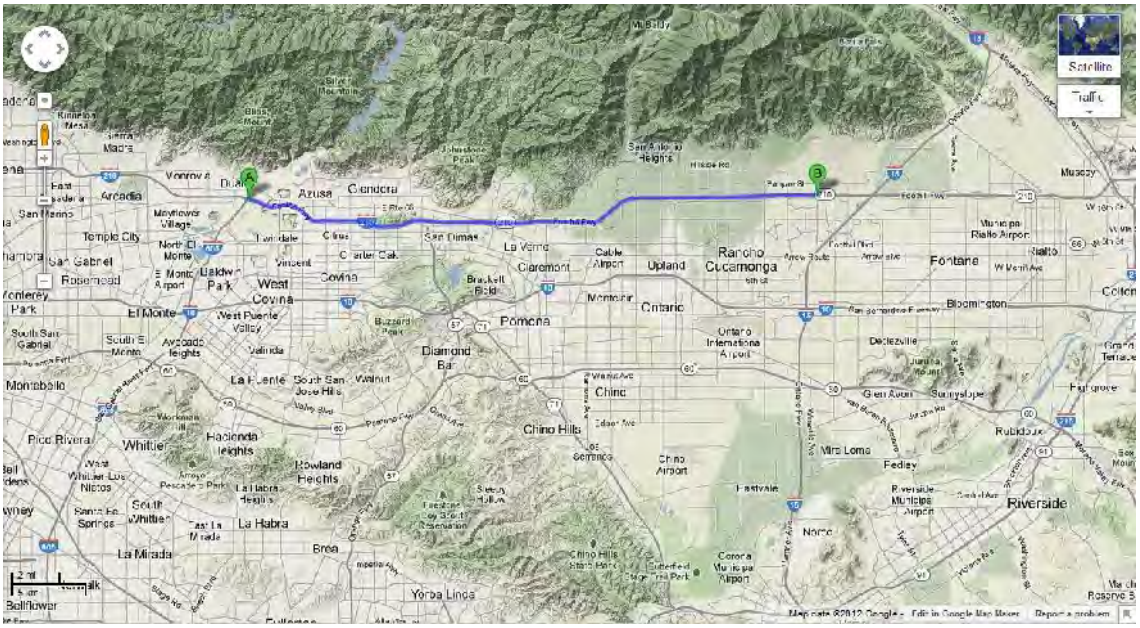

FIGURE 4 Example trip used for velocity trajectory synthesis.

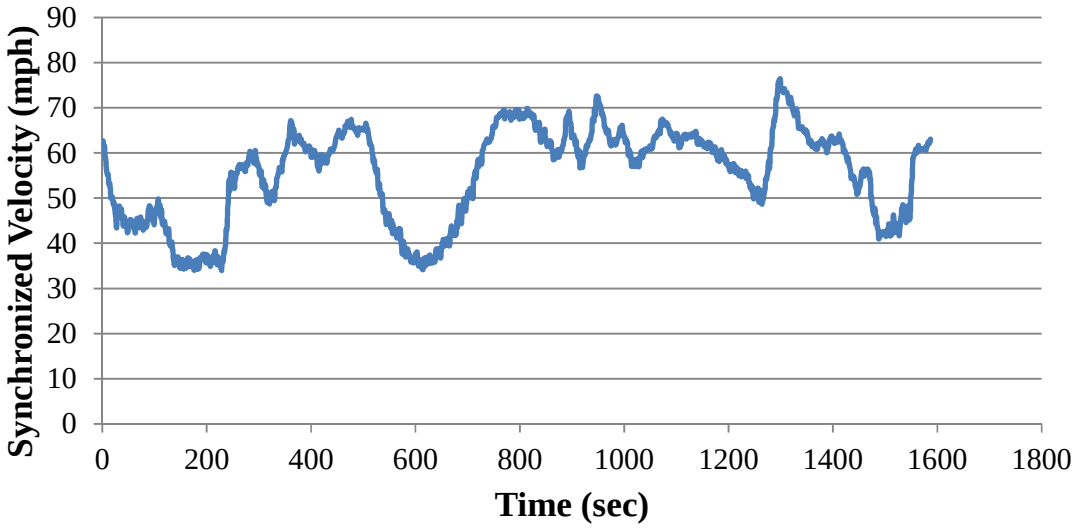

FIGURE 5 Synthesized velocity trajectory for the example trip starting at 16:00 on January 17th, 2012.

ROAD GRADE INFORMATION SYNCHRONIZATION

The road grade information associated with the synthesized velocity trajectory can be obtained from Dynamic Roadway Network (DynaNet) (*28*). However, such road grade information is location-based. For different driving cycles, time-based road grade information (i.e., second-by-second road grade) needs to be obtained by synchronizing with the vehicle velocity at each time step. Figure 6 shows both location-based and time-based road grade profiles for the aforementioned example.

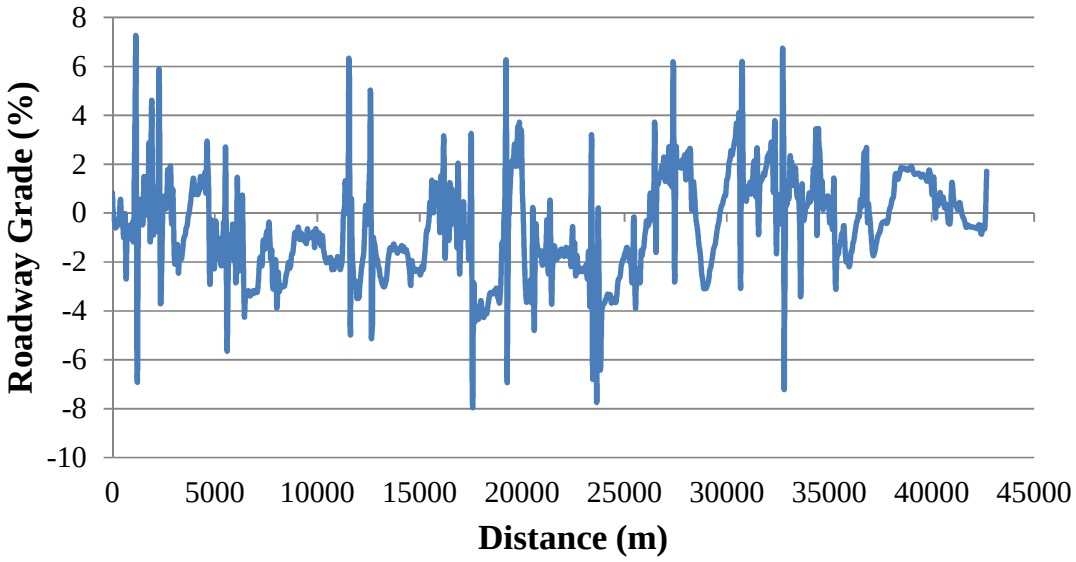

(a) Location-based road grade (%)

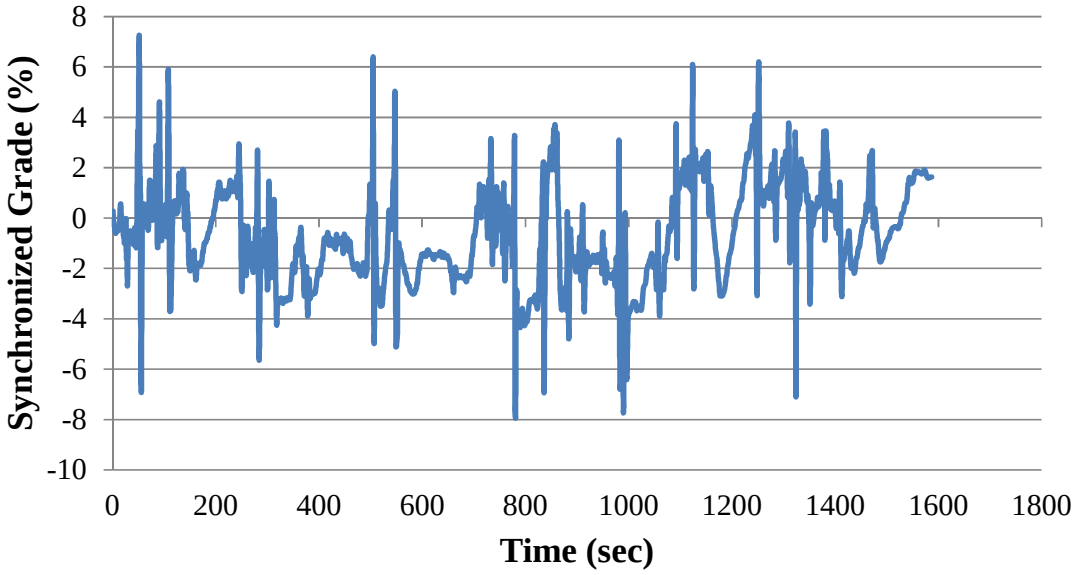

(b) Time-based road grade (%) after synchronization with the associated trip

FIGURE 6 Synchronized road grade profile for the synthesized velocity trajectory along I-210 E, CA, starting at 16:00 on January 17th, 2012.

PHEV MODELING

Several approaches with different levels of complexity have been proposed for modeling PHEV vehicle and powertrain. A complex PHEV model with a large number of states may not be suitable for the optimization of PHEV energy control. Therefore, a simplified but sufficiently detailed vehicle and powertrain model was developed in this study. In general, there are three major PHEV powertrain architectures: a) series, b) parallel, and c) power-split (series-parallel).This study is focused on the power-split one. Figure 7 depicts the configuration of a power-split PHEV, in which three major sub-systems: a) internal combustion engine (ICE), b) planetary gear set (PGS), and c) motor/battery are modeled as described below.

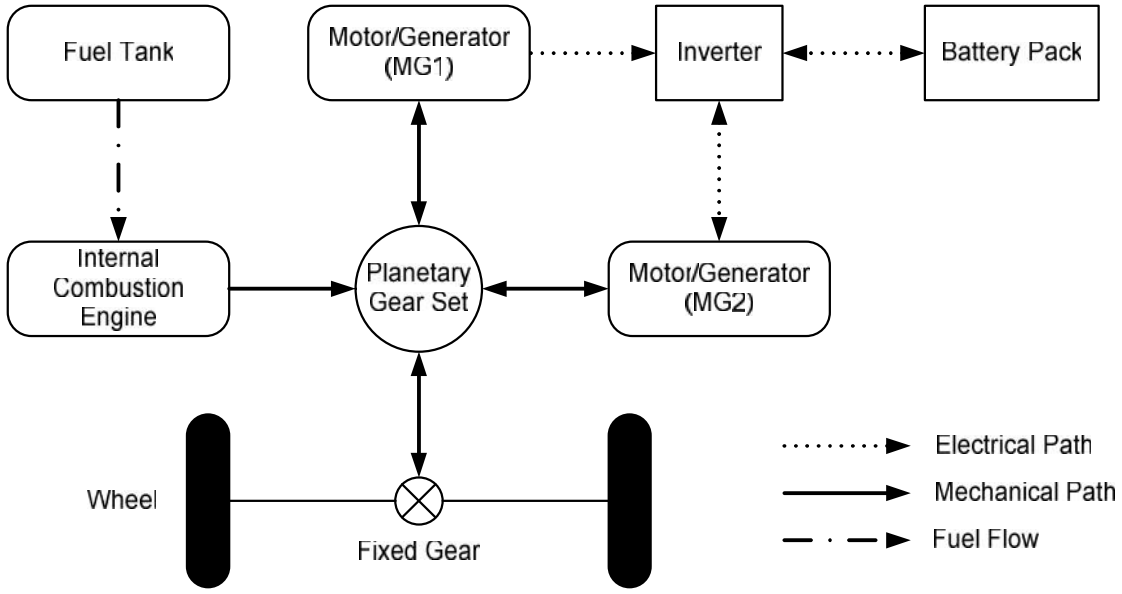

FIGURE 7 Power-split plug-in hybrid electric vehicle configuration.

Internal Combustion Engine

To simplify the whole PHEV model, the engine dynamics were ignored based on the quasi-static assumption (*29*). Fuel consumption and engine-out emissions wre considered as static functions of two independent variables: engine speed and engine torque. Based on the archived data in Autonomie simulation tool (*30*), the engine efficiency map and brake specific fuel consumption (BSFC) map of a mid-size, two-wheel drive PHEV with power-split architecture were extracted. In addition, it is assumed that the engine is fully warmed up; hence, engine temperature effect is not considered.

Planetary Gear Set

One of the major components in a power-split PHEV is the power split device, also known as the planetary gear set (PGS), which consists of a ring gear, a sun gear, a carrier gear and several pinion gears (see Figure 8). More specifically, the sun gear is connected to a motor/generator (MG1), which is used to assist the engine start and charge the battery pack by transferring energy from the engine during normal driving. The carrier gear is attached to the engine. The ring gear is linked to the drive shaft and the other motor/generator (MG2), which enables direct motor propulsion and energy restoration due to regenerative braking. By lever analogy, the relationship among the angular velocities of different components in PGS can be derived as

$$\omega_S \cdot S + \omega_R \cdot R = \omega_C \cdot (S + R) \tag{8.a}$$

or,

$$\omega_S \cdot N_S + \omega_R \cdot N_R = \omega_C \cdot (N_S + N_R) \tag{8.b}$$

Note that MG1, ICE and MG2 are attached to the sun gear, carrier gear, and ring gear, respectively, i.e.,

$$\omega_{MG1} = \omega_S \tag{8.c}$$
$$\omega_{ICE} = \omega_C \tag{8.d}$$
$$\omega_{MG2} = \omega_R \tag{8.e}$$

Therefore,

$$\omega_{MG1} \cdot S + \omega_{MG2} \cdot R = \omega_{ICE} \cdot (S + R) \tag{8}$$

where S and R are the radii of the sun gear and ring gear, respectively; N_S and N_R are the numbers of teeth of the sun gear and ring gear, respectively; ω_S, ω_C, and ω_R represent the angular velocities of sun gear, carrier gear, and ring gear, respectively; and ω_{MG1}, ω_{ICE}, and ω_{MG2} denote the angular velocities of MG1, ICE, and MG2, respectively. Since the ring gear is connected to the vehicle drive axle with a fixed transmission ratio, N_f, the angular velocity of the wheel, ω_{wh}, is

$$\omega_{wh} = \omega_{MG2}/N_f \tag{9}$$

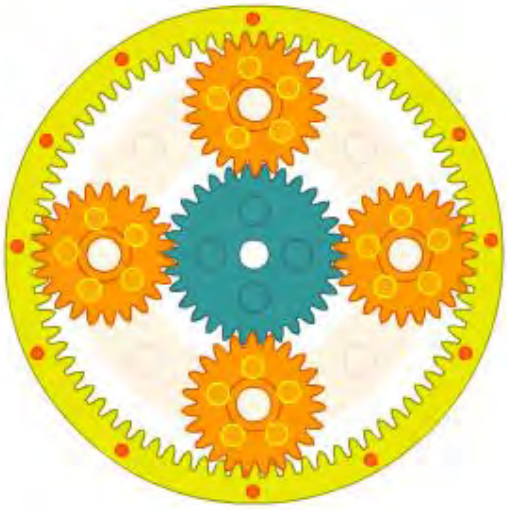

FIGURE 8 Power split device [Source: http://eahart.com/prius/psd/].

If it is further assumed that

1) The inertia of pinion gears are trivial;
2) Gear mechanical efficiency is perfect;
3) There is no efficiency loss in the driveline;
4) Only the vehicle longitudinal dynamics is considered; and
5) There is no tire slip;

then the following dynamic equations for each part of PGS can be derived based on the conservation of angular momentum:

On the sun gear shaft,

$$\dot{\omega}_S \cdot I_S = F_{int} \cdot S + T_S \tag{10.a}$$

and

$$\dot{\omega}_{MG1} \cdot I_{MG1} = T_{MG1} - T_S \tag{10.b}$$

From Equation (8.c), (10.a), and (10.b),

$$\dot{\omega}_{MG1} \cdot (I_S + I_{MG1}) = F_{int} \cdot S + T_{MG1} \tag{10}$$

where I_S and I_{MG1} are the inertias of the sun gear and MG1, respectively; F_{int} is the internal force on the pinion gears; and T_S and T_{MG1} are the torques applied to the sun gear and MG1, respectively.

On the carrier gear shaft,

$$\dot{\omega}_C \cdot I_C = T_C - (F_{int} \cdot S + F_{int} \cdot R) \tag{11.a}$$

and

$$\dot{\omega}_{ICE} \cdot I_{ICE} = T_{ICE} - T_C \tag{11.b}$$

From Equation (8.b), (11.a) and (11.b),

$$\dot{\omega}_{ICE} \cdot (I_C + I_{ICE}) = T_{ICE} - (F_{int} \cdot S + F_{int} \cdot R) \quad (11)$$

where I_C and I_{ICE} are the inertias of the carrier gear and ICE, respectively; and T_C and T_{ICE} are the torques applied to the carrier gear and ICE, respectively.

On the ring gear shaft,

$$\dot{\omega}_R \cdot I_R = F_{int} \cdot R + T_R \quad (12.a)$$

and

$$\dot{\omega}_{wh} = (T_{wh} - T_{rl})/(M_r \cdot R_t^2) \quad (12.b)$$

where I_R is the inertia of the ring gear and T_R is the associated torque; R_t is the tire radius; $M_r = M_{veh} + J_r/R_t^2$ is the effective mass of the vehicle given that M_{veh} is the vehicle mass and J_r is the equivalent moment of inertia of the rotating components in the vehicle; T_{rl} is the torque due to road loads; and $T_{wh} = T_{pr} - T_{br}$ is the net wheel torque given that T_{pr} and T_{br} are the final propulsion torque after transmission and the friction brake toque, respectively. According to Figure 7,

$$T_{pr} = (T_{MG2} - \dot{\omega}_{MG2} \cdot I_{MG2} - T_R) \cdot N_f \quad (12.c)$$

As to T_{rl}, it consists of three types of torque: a) rolling resistance torque, T_{rr}, b) climbing torque, T_{cl}, and c) aerodynamic drag torque, T_{ad}, i.e.,

$$T_{rl} = T_{rr} + T_{cl} + T_{ad} \quad (12.d)$$

More specifically,

$$T_{rr} = M_{veh} \cdot g \cdot cos(\alpha) \cdot C_r \cdot R_t \quad (12.e)$$
$$T_{cl} = M_{veh} \cdot g \cdot sin(\alpha) \cdot R_t \quad (12.f)$$
$$T_{ad} = 0.5 \cdot \rho \cdot A \cdot C_d \cdot v_{veh}^2 \cdot R_t \quad (12.g)$$

where g is the gravitational acceleration (9.81 m/s^2); C_r is the rolling resistance coefficient; α is the road grade; ρ is the density of air; A is the vehicle frontal area; and C_d is aerodynamic drag coefficient.

Also note that

$$v_{veh} = \omega_{wh} \cdot R_t \quad (12.h)$$

From Equation (1.c), (2), and (5.a) – (5.h),

$$\dot{\omega}_{MG2} \cdot \left(R_t^2/N_f \cdot M_r + I_{MG2} \cdot N_f + I_R \cdot N_f\right) = (T_{MG2} + F_{int} \cdot R) \cdot N_f - T_{br} - \left[M_{veh} \cdot g \cdot cos(\alpha) \cdot C_r - M_{veh} \cdot g \cdot sin(\alpha) - 0.5 \cdot \rho \cdot A \cdot C_d \cdot \left(\omega_{MG2} \cdot R_t^2/N_f\right)^2\right] \cdot R_t \quad (12)$$

It should be pointed out that the positive directions for both T and ω in the

equations above are as shown in Figure 9.

Furthermore, Equations (8) and (10) – (12) can be written in the matrix form as follows:

$$\begin{bmatrix} S & -(R+S) & R & 0 \\ I_{MG1}+I_S & 0 & 0 & -S \\ 0 & I_{ICE}+I_C & 0 & S+R \\ 0 & 0 & R_{tire}^2/N_f \cdot M_r + I_{MG2} \cdot N_f + I_R \cdot N_f & -R \cdot N_f \end{bmatrix} \begin{bmatrix} \dot{\omega}_{MG1} \\ \dot{\omega}_{ICE} \\ \dot{\omega}_{MG2} \\ F_{int} \end{bmatrix} =$$

$$\begin{bmatrix} 0 \\ T_{MG1} \\ T_{ICE} \\ T_{MG2} \cdot N_f - T_{br} - M_{veh} \cdot g \cdot cos(\alpha) \cdot C_r \cdot R_t - M_{veh} \cdot g \cdot sin(\alpha) \cdot R_t - 0.5 \cdot \rho \cdot A \cdot C_d \cdot \left(\omega_{MG2}/N_f\right)^2 \cdot R_t^3 \end{bmatrix} \quad (13)$$

The number of mechanical degrees of freedom is 2 in the above system, where ω_{ICE} and ω_{MG2} are selected as the state variables.

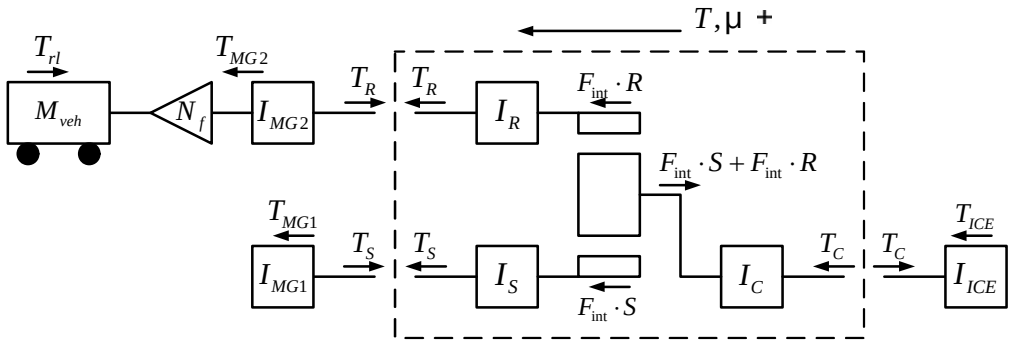

FIGURE 9 Free body diagram for the mechanical path of PHEV.

Motor/Battery

The inverter is used to draw/store power from/into the battery batch. The relationship among the battery state of charge (SOC), the battery capacity, and the current can be described as

$$\dot{SOC} = -I_b(t)/C_{max} \quad (14)$$

where $I_b(t)$ and C_{max} are the battery current at time t and the maximum capacity, respectively. For simplicity, the battery is modeled as a series circuit with an internal resistor R_b and open circuit voltage V_{OC} (see Figure 10). In this study, a finite battery charge capacity model is used as the energy storage system, where the voltage source is charge-dependent (*31*).

The battery power is given by

$$P_b(t) = I_b(t) \cdot (V_{OC}(t) - I_b(t) \cdot R_b) \quad (15)$$

or

$$I_b(t) = \left(V_{OC}(t) - \sqrt{V_{OC}^2(t) - 4 \cdot R_b \cdot P_b(t)}\right)/(2 \cdot R_b) \quad (16)$$

Note that if P_b and I_b are positive, the battery is discharged. If they are negative, the battery is charged. The relationship of the power flows among the battery and the electric motors/generators through the inverter is governed by

$$P_b(t) = T_{MG1} \cdot \omega_{MG1} \cdot \eta_{MG1}^k \cdot \eta_{i1}^k + T_{MG2} \cdot \omega_{MG2} \cdot \eta_{MG2}^k \cdot \eta_{i2}^k \quad (17)$$

where η_{MG1} and η_{MG2} are the efficiencies of MG1 and MG2, respectively, which can be obtained from the electric motor efficiency maps in Autonomie; and η_{i1} and η_{i2} are the corresponding efficiencies of the inverters. The exponent *k* is 1 if the battery is being charged by the generators and -1 if the battery is charging the electric motors.

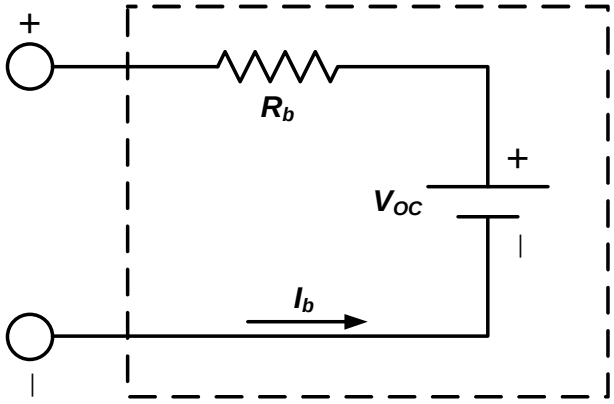

FIGURE 10 Internal resistance battery model.

According to Equation (7) through (10), SOC can be derived as

$$\dot{SOC} = -\left(V_{OC} - \sqrt{V_{OC}^2 - 4 \cdot R_b \cdot (T_{MG1} \cdot \omega_{MG1} \cdot \eta_{MG1}^k \cdot \eta_{i1}^k + T_{MG2} \cdot \omega_{MG2} \cdot \eta_{MG2}^k \cdot \eta_{i2}^k)}\right)/(2 \cdot R_b \cdot C_b) \quad (11)$$

PHEV Model Parameters

All major parameters and the associated values of the PHEV model used in this study are listed in Table 1.

TABLE 1 List of PHEV Model Parameters

Parameters	Value	Unit
Vehicle curb weight	1718	kg
Final drive ratio	3.93	/
Vehicle equivalent mass	1853	kg
Tire radius	0.317	m
No. of teeth on sun gear	30	/
No. of teeth on ring gear	78	/
Gravitational acceleration	9.81	m/s^2
Rolling resistance coefficient (constant term)	0.008	
Rolling resistance coefficient (linear term)	0.00012	s/rad
Air density	1.2041	kg/m^3
Projected frontal area	2.2508	m^2
Aerodynamic drag coefficient	0.26	
Maximum engine power	60	kWatt
Moment of inertia for engine	0.1598	$kg*m^2$
Maximum motor power	50	kWatt
Moment of inertia for motor	0.0302	$kg*m^2$
Maximum generator power	30	kWatt
Moment of inertia for generator	0.0287	$kg*m^2$
Maximum brake torque	2000	N*m
No. of battery cells per module	12	/
No. of battery module	6	/
Nominal open-circuit voltage	3.6	volt
Battery capacity	17	Ah
Minimum state of charge (SOC)	0.2	/

OPTIMAL CHARGE-DEPLETING CONTROL

Given a synthesized velocity trajectory and corresponding road grade information, the required power at wheel at each time step can be calculated based on vehicle dynamics. Based on the simplified PHEV model described in the previous section, the feasible sets of engine power supply and the associated drop or gain in the batter SOC can be obtained at each time step. Therefore, the optimal charge-depleting control problem for PHEV can be formulated as a 0-1 binary mixed integer non-linear programming (MINLP) as follows:

$$\min \sum_{k=1}^{T} \sum_{i=1}^{N} x(k,i) \cdot \frac{P_i^{eng}}{\eta_i^{eng}} \tag{13}$$

Subject to

$$\sum_{k=1}^{j} f_k\left(P_k - \sum_{i=1}^{N} x(k,i) \cdot P_i^{eng}\right) \le C \qquad \forall j = 1, \dots, T \tag{14}$$

$$\sum_{i=1}^{N} x(k,i) = 1 \qquad \forall k \tag{15}$$

$$x(k,i) = \{0,1\} \qquad \forall k,i \tag{16}$$

where T is the time span (say, 1800 sec) for the whole trip; N is the number of discretized power level for the engine C is the threshold for the gap of battery's state of charge between the initial and the minimum; P_i^{eng} is the i-th discretized power level for the engine and η_i^{eng} is the associated engine efficiency; and P_k is the required power at wheel from the vehicle; f_k is a non-linear function to calculate the falls and rises of battery SOC, ΔSOC (positive for discharging whereas negative for charging), based on the simplified PHEV model. If ΔSOC is calculated for each associated engine power level at each time step, then constraint (14) can be replaced by

$$SOC^{ini} - SOC^{max} \leq \sum_{k=1}^{j} x(k,i) \cdot \Delta SOC(k,i) \leq SOC^{ini} - SOC^{min} \qquad \forall i, j = 1, \dots, T \tag{17}$$

where SOC^{ini} is the initial SOC; and SOC^{min} and SOC^{max} are the minimum and maximum of SOC, respectively. Therefore, the problem is turned into a mixed integer linear programming (MILP) and numerous efficient solvers can be applied to obtain the global optimal solution. In this study, we used IBM ILOG CPLEX Optimization Studio (ver. 12.2) to solve the proposed MILP problem.

The trip-based optimization problem formulation above can be extended to a tour-based one that considers battery recharging opportunities at intermediate stops in the tour as follows:

$$\min \sum_{l=1}^{M} \sum_{k=1}^{T_l} \sum_{i=1}^{N} x(k,i,l) \cdot \frac{P_i^{eng}}{\eta_i^{eng}} \tag{18}$$

Subject to

$$SOC_l^{ini} - SOC^{max} \leq \sum_{k=1}^{j} x(k,i,l) \cdot \Delta SOC(k,i,l) \leq SOC_l^{ini} - SOC^{min} \qquad \forall i, l, j = 1, \dots, T_l \tag{19}$$

$$SOC_l^{ini} - \sum_{k=1}^{T_l} x(k,i,l) \cdot \Delta SOC(k,i,l) + SOC_l^{rec} = SOC_{l+1}^{ini} \qquad \forall l \tag{20}$$

$$\sum_{i=1}^{N} x(k,i,l) = 1 \qquad \forall k, l \tag{21}$$

$$x(k,i,l) = \{0,1\} \qquad \forall k, i, l \tag{22}$$

where l is the trip index within a tour; and SOC_l^{rec} represents the gain of SOC at the end of l-th trip due to batter recharging. It is still an MILP and can be solved very efficiently using CPLEX.

EVALUATION OF INTELLIGENT ENERGY MANAGEMENT STRATEGY

Trip-Based Control Evaluation

The proposed intelligent energy management strategy using MILP for optimal

charge-depleting control was applied to the example trip shown in Figure 4 as well as the trip in an opposite direction, i.e., from Day Creek Blvd. to Interchange of I-210 and I-605 (along I-210 W) in Southern California, starting at 08:00 on January 17th, 2012. Figure 11 presents the SOC profiles along those trips whose initial SOC and minimum SOC are 0.8 (also the maximum SOC in the normal operating range) and 0.2, respectively. For comparison, Figure 12 illustrates the results using the binary (CD-CS) mode as the energy management strategy. According to Table 2, the proposed strategy can save fuel consumption by 14.4% on the westbound trip and 9.3% on the eastbound trip compared to the binary-mode strategy.

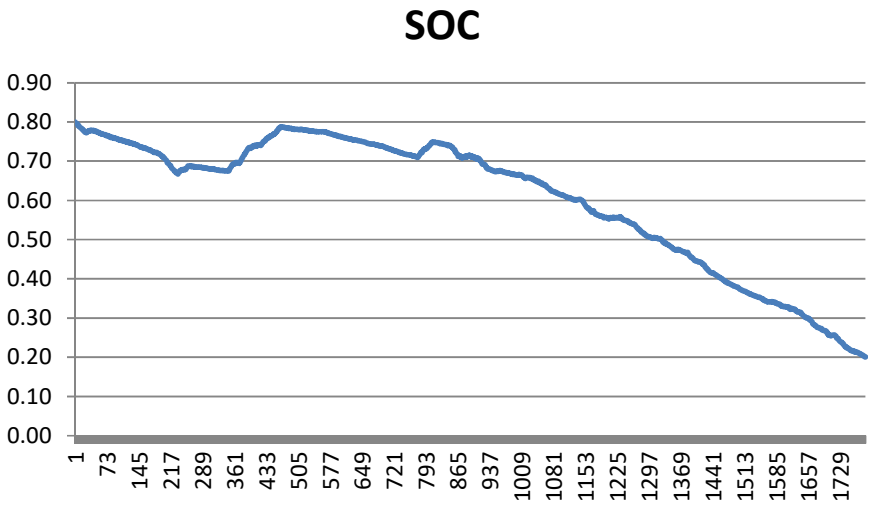

(a) PHEV's SOC profile for I-210W sample trip (starting at 08:00)

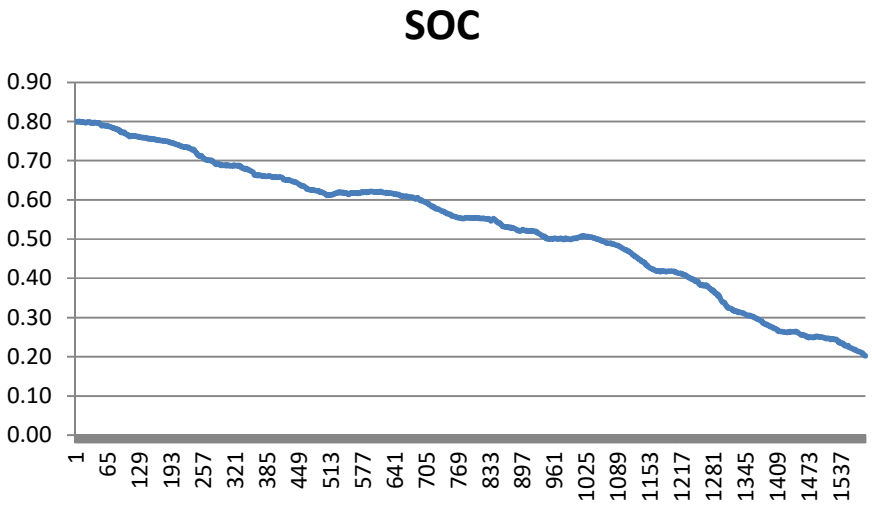

(b) PHEV's SOC profile for I-210E sample trip (starting at 16:00)

FIGURE 11 Results of intelligent energy management strategy.

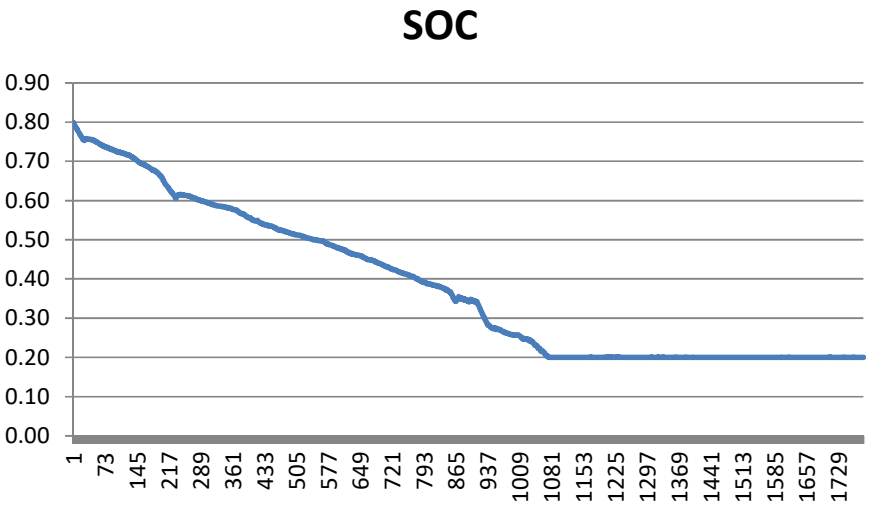

(a) PHEV's SOC profile for I-210W sample trip (starting at 08:00)

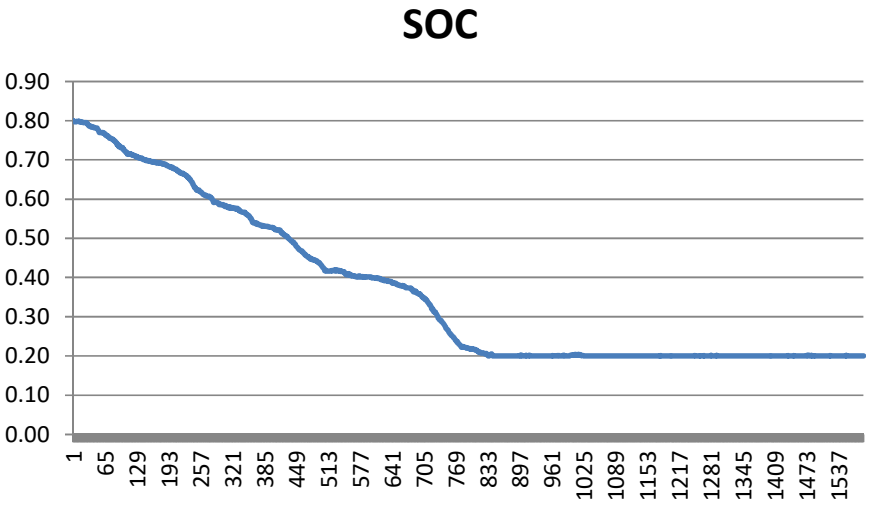

(b) PHEV's SOC profile for I-210E sample trip (starting at 16:00)

FIGURE 12 Results of binary-mode energy management strategy.

TABLE 2 Total Trip Fuel Consumption for Trip-Based Control

Trip	Fuel Consumption (gallons)		
	Proposed Strategy	Binary Mode Strategy	% Difference
I-210 W starting at 08:00	0.346	0.404	14.4
I-210 E starting at 16:00	0.311	0.343	9.3

Tour-Based Control Evaluation

To evaluate the proposed intelligent energy management strategy at the tour level, a hypothetic trip chain was set up as follows:

a) Trip #1: From Day Creek Blvd. to Interchange of I-210 and I-605 (along I-210 W), CA, starting at 08:00 on January 17th, 2012. This trip is mainly downhill;
b) Trip #2: From Interchange of I-210 and I-605 (along I-210 E) to Day Creek Blvd., starting at 16:00 on January 17th, 2012. This trip is mainly uphill;
c) Between the end of Trip #1 and the beginning of Trip #2, there is a battery recharging opportunity to gain SOC by 60% (i.e., $SOC_1^{rec} = 0.6$).

Figure 13(a) presents the SOC profile along the whole tour using the tour-based optimal energy management strategy with the knowledge of recharging opportunity of 60% SOC recovery at the end of Trip #1. Due to such knowledge, the SOC at the end of Trip #1 (downhill route) reached the minimum SOC of 0.2.

For comparison, the following two other scenarios were considered:

1) Using tour-based optimal energy management strategy without the knowledge of battery recharging opportunity. The SOC profile for this scenario is shown in Figure 13(b);
2) Using the binary-mode energy management strategy (no matter whether the battery recharging opportunity is known). Figure 13(c) illustrates the results for this scenario.

As shown in Figure 13(b), the SOC at the end of Trip #1 was 0.46 rather than 0.2. Since it was unknown how much SOC could be gained before the beginning of Trip #2, the control strategy attempted to reserve battery energy for the return trip. Due to the lack of knowledge about the battery recharging opportunity, the strategy over-reserved the battery energy and did not fully take advantage of available energy by electrical grids (since SOC can only be gained up to a maximum limit; 0.8 in this study). It is interesting to find that such scenario inadvertently resulted in even higher fuel consumption than the binary-mode strategy whose SOC profile is shown in Figure 13(c). Based on the total fuel consumption results for the example tour in Table 3, the tour-based control strategy, when used in conjunction with information about battery recharging opportunity, have 14.9% lower total fuel consumption than the tour-based strategy without such information, and 12.1% lower total fuel consumption than the binary mode strategy.

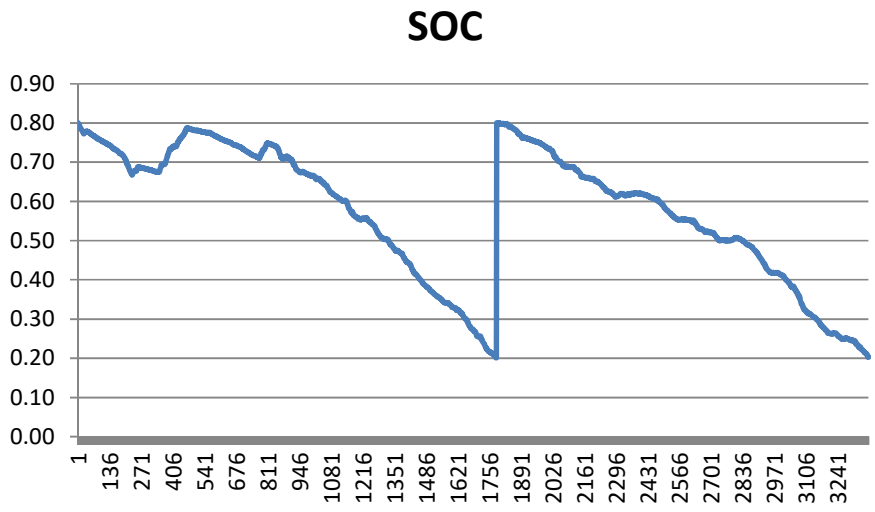

(a) Optimal strategy with knowledge of rechargeable opportunity

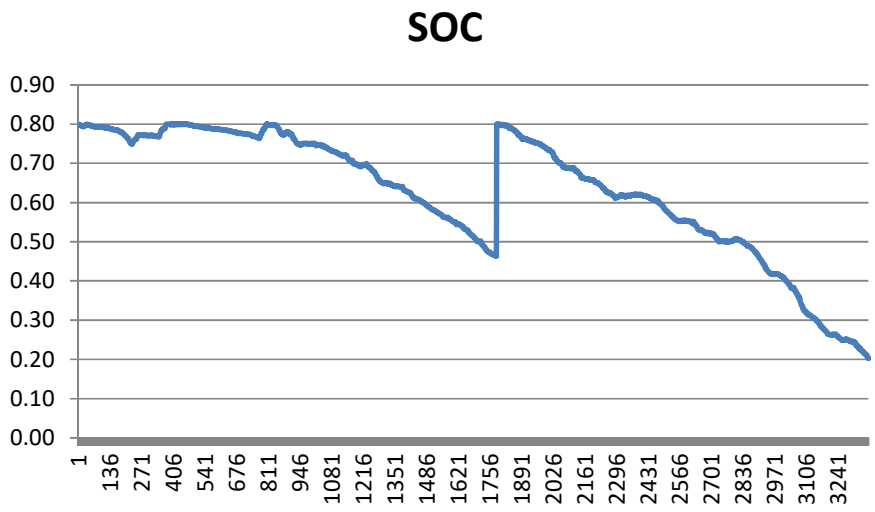

(b) Optimal strategy without knowledge of rechargeable opportunity

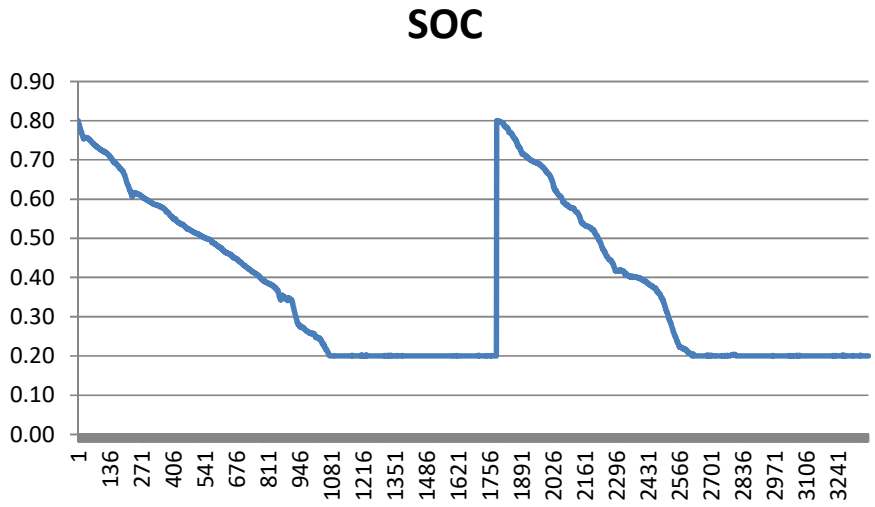

(c) Binary-mode strategy

FIGURE 13 PHEV's SOC profile for a sample tour.

TABLE 3 Total Tour Fuel Consumption for Tour-Based Control (in gallon)

		Battery Recharging Opportunity	
		Known	Unknown
Charge-Depleting Control	Proposed Strategy	0.657	0.772
	Binary Mode Strategy	0.747	0.747

CONCLUSIONS AND FUTURE WORK

In this study, we proposed an intelligent energy management strategy for PHEVs. At the trip level, the strategy takes into account *a priori* knowledge of vehicle location, roadway characteristics, and real-time traffic information on the travel route from intelligent transportation system technologies in generating synthesized velocity trajectory for the trip. The synthesized velocity trajectory is then used to determine charge-depleting control that is formulated as a mixed integer linear programming to minimize the total fuel consumption for the trip. The strategy can be extended to optimize fuel consumption at the tour level if a pre-planned travel itinerary for the tour and the information about available battery recharging opportunities at intermediate stops in the tour are available. The effectiveness of the proposed strategy, both for the trip-based and tour-based controls, was evaluated against the existing binary mode energy management strategy using a real-world example trip/tour in Southern California. The evaluation results show that the fuel savings of the proposed strategy over the binary mode strategy are around 10-15%.

There are several topics for future work on this research. For instance, the velocity trajectory synthesis method could be improved by imposing a vehicle power constraint in order to avoid having parts of the velocity trajectory requiring power beyond the physical limit of the vehicle. The optimal charge-depleting control could be formulated and solved by other forms of optimization techniques such as dynamic programing. In additional, the further evaluation of the trip-based and tour-based controls using additional data sets, the sensitivity analysis of critical control parameters, and the implementation of the proposed strategy on a test PHEV would all make an interesting and worthwhile future research topic as well.

ACKNOWDGEMENT

The authors gratefully acknowledge the support from the University of California Transportation Center (UCTC). We would like to thank Joseph Menke for his contribution to the study. We also thank Dr. George Scora (UC Riverside), Dr. Jing-Quan Li (UC Berkeley), Prof. Huei Peng (U. of Michigan), and Yiming He (Clemson U.) for constructive discussion and comments during the study.

REFERENCES

1. Bureau of Transportation Statistics (BTS). http://www.bts.gov/publications/national_transportation_statistics, accessed on February 20th, 2012
2. U.S. Environmental Protection Agency (EPA). *Inventory of U.S. greenhouse gas emissions and sinks: 1990 – 2009*. Final report, EPA 430-R-11-005, April, 2011
3. He, Y., R. Jackeline, M. Chowdhury, P. Pierluigi, and P. Bhavsar. Forward Power-Train Energy Management Modeling for Assessing Benefits of Integrating Predictive Traffic Data into Plug-in Hybrid Electric Vehicles. Transportation Research Part D, 17(3), 2012, pp. 201 – 207
4. Gong, Q., Y. Li, Z-R Peng. *Power Management of Plug-in Hybrid Electric Vehicles Using Neural Network Based Trip Modeling*. In Proceedings of the American Control Conference, June 2009, pp. 4601-4606
5. Gong, Q., Y. Li and Z-R Peng. *Trip-Based Optimal Power Management of Plug-in Hybrid Electric Vehicles*. IEEE Transactions on Vehicular Technology, Vol. 57, No. 6, Nov, 2008, pp. 3393-3401
6. Zhang, C., A. Vahidi, X. Li and D. Essenmacher. *Role of Trip Information Preview in Fuel Economy of Plug-in Hybrid Vehicles*. Proceedings of the ASME 2009 Dynamic Systems and Control Conference, October, 2009, Hollywood, California, USA.
7. Zhang, C., A. Vahidi. Real-Time Optimal Control of Plug-in Hybrid Vehicles with Trip Preview. Proceedings of American Control Conference, Baltimore, MD, USA, June, 2010, pp. 6917-6922
8. Duoba, M.. *Evaluating PHEV Technology Using Component HIL, Subsystem, and Chassis Dynamometer Testing: Methods and Results*. Proceedings of the SAE Hybrid Vehicle Technology Symposium, San Diego, CA, February 7 – 8, 2007
9. Chen, C., A. Skabardonis, and P. Varaiya. *Travel Time Reliability as a Measure of Service*. Transportation Research Record, No. 1855, 2003, pp. 74 – 79
10. Rice, J. and E. Van Zwet. *A Simple and Effective Method for Predicting Travel Times on Freeways*. IEEE Transactions on Intelligent Transportation Systems, Vol. 5, No. 3, 2004, pp. 200 – 207
11. Ni, D. and H. Wang. *Trajectory Reconstruction for Travel Time Estimation*. Journal of Intelligent Transportation Systems, Vol. 12, No. 3, 2008 pp. 113 – 125
12. Krol, L.. *The Reconstruction of Vehicle Trajectories with Dynamic Macroscopic Data*. Master Thesis, University of Twente, The Netherlands, 2009
13. Herrera, J. and A. Bayen. *Traffic Flow Reconstruction Using Mobile Sensors and Loop Detector Data*. In 87th TRB Annual Meeting, Transportation Research Board, Washington D. C., January, 2008
14. Barth, M. J., E. Johnston and R. R. Tadi. *Using GPS Technology to Relate Macroscopic and Microscopic Traffic Parameters*. Transportation Research Record, No. 1520, 1996, pp. 89 – 96
15. Lin, J. and D. A. Niemeier. *Estimating Regional Air Quality Vehicle Emission Inventories: Constructing Robust Driving Cycles*. Transportation Science, Vol. 37, No. 3, 2003, pp. 330 – 346

16. Liu, J., H. Peng, and Z. Filipi. *Modeling and Analysis of the Toyota Hybrid System*. Proceedings of the IEEE/ASME International Conference on Advanced Intelligent Mechatronics, Monterey, 2005
17. Burke, A., and E. V. Gelder. *Plug-in Hybrid-Electric Vehicle Powertrain Design and Control Strategy Options and Simulation Results with Lithium-ion Batteries*. EET-2008 European El-Drive Conference international Advanced Mobility Forum, Geneva, Switzerland, March, 2008
18. Musardo, C., G. Rizzoni, Y. Guezennec, B. Staccia. *A-ECMS: An Adaptive Algorithm for Hybrid Electric Vehicle Energy Management*. European Journal of Control, Vol. 11, No. 4-5, 2005, pp. 509 – 524
19. Perez, L. V., G. R. Bossio, D. Moitre, and G. O. Garcia. *Optimization of Power Management in an Hybrid Electric Vehicle Using Dynamic Programming*. Mathematics and Computers in Simulation, Vol. 73, 2006, pp. 244 – 254
20. Karbowski, D., A. Rousseau, S. Pagerit, and P. Sharer. *Plug-in Vehicle Control Strategy: from Global Optimization to Real-time Application*. In Electric Vehicle Symposium, EVS22. Yokohama, 2006
21. Lin, C., H. Peng, J. W. Griizzle, J. Kang. *Power Management Strategy for a Parallel Hybrid Electric Truck*. IEEE Transactions on Control Systems Technology, Vol. 11, 2003, No. 6, pp.
22. Liu, J. and H. Peng. *Modeling and Control of A Power-split Hybrid Vehicle*. IEEE Transactions on Control Systems Technology, Vol. 16, No. 6, 2008, pp. 1242 – 1251
23. Tulpule, P., V. Marano, and G. Rizzoni. *Effects of Different PHEV Control Strategies on Vehicle Performance*. In Proceedings of the American Control Conference, June 2009, pp. 3950-3955
24. Devault, R. C.. *"Just-in-Time" Battery Charge Depletion Control for PHEVs and E-REVs for Maximum Battery Life*. SAE world congress 2009.
25. He, Y., M. Chowdhury, P. Pisu, and Y. Ma. *An Energy Optimization Strategy for Power-split Drivetrain Plug-in Hybrid Electric Vehicles*. Transportation Research Part C, Vol. 22, 2012, pp. 29 – 41
26. Environmental Protection Agency. *MOVES2010 Highway Vehicle: Population and Activity Data*. November, 2010
27. Van Lint, J. and N. van der Zijpp. *Improving a Travel Time Estimation Algorithm by Using Dual Loop Detectors*. Transportation Research Record, No. 1855, 2003, pp. 41 – 48
28. Boriboonsomsin, K., Barth, M., Zhu, W., and Vu. A. (2010). ECO-routing navigation system based on multi-source historical and real-time traffic information. Proceedings of the 13th International IEEE Conference on Intelligent Transportation Systems, Madeira Island, Portugal, September 19-22.
29. Kolmanovsky, I., M. Nieuwstadt, and J. Sun. *Optimization of Complex Powertrain Systems for Fuel Economy and Emissions*. Proceedings of IEEE International Conference on Control Applications, Hawaii, 1999
30. Argonne National Laboratory. *AUTONOMIE*, http://www.autonomie.net/. Accessed on February 16th, 2012.
31. MathWorks. MATLAB R2010b, 2011.